J. Cent. South Univ. (2015) 22: 3097−3107
DOI: 10.1007/s11771-015-2846-6

Springer

Numerical simulation of triaxial compression test for brittle rock sample using a modified constitutive law considering degradation and dilation behavior

TAN Xin(谭鑫)[1, 2], KONIETZKY H[2], FRÜHWIRT T[2]

1. College of Civil Engineering, Hunan University, Changsha 410082, China;
2. Geotechnical Institute, TU Bergakademie Freiberg, Freiberg 09599, Germany

Abstract: The understanding of the rock deformation and failure process and the development of appropriate constitutive models are the basis for solving problems in rock engineering. In order to investigate progressive failure behavior in brittle rocks, a modified constitutive model was developed which follows the principles of the continuum damage mechanics method. It incorporates non-linear Hoek-Brown failure criterion, confining pressure-dependent strength degradation and volume dilation laws, and is able to represent the nonlinear degradation and dilation behaviors of brittle rocks in the post-failure region. A series of triaxial compression tests were carried out on Eibenstock (Germany) granite samples. Based on a lab data fitting procedure, a consistent parameter set for the modified constitutive model was deduced and implemented into the numerical code FLAC^{3D}. The good agreement between numerical and laboratory results indicates that the modified constitutive law is well suited to represent the nonlinear mechanical behavior of brittle rock especially in the post-failure region.

Key words: progress failure; strength degradation; dilation; Hoek-Brown criterion; numerical simulation; brittle rock

1 Introduction

The mechanical response of rocks during compressive loading processes contains several different phenomena, like elastic deformation, stress propagation and redistributions, micro fracture initiation and propagation, crack coalescence and finally macroscopic failure. Whereas the pre-failure region is characterized by elastic response, some subcritical crack growth and micro-cracking, the post-failure region of brittle rocks is characterized by massive crack propagation and coalescence and finally the localization into shear bands. Associated with these processes, non-linear macroscopic fracture behaviors and volumetric dilatancy appear. Additionally, all of these processes and behaviors are greatly influenced by confining pressure. Ideally, all these mechanical behaviors should be represented by certain kinds of comprehensive constitutive models. In the late 1950s, researchers started to apply plastic theory in constitutive model to rock materials. The elastic-perfectly plastic model and the Mohr-Coulomb failure criterion became a widely adopted constitutive model. Later on, the continuous damage mechanics (CDM) model has emerged as an effective method for modelling the failure of rock materials, which is based on damage analysis. The internal state variables are used in CDM motheds to relate the effect of microdefects to the macroscopic material properties [1−4].

YUAN and HARRISON [5] presented a review of continuous damage mechanics methods and pointed out that this phenomenological models are based on purely macroscopic considerations of the material during damage evolution, irrespective of microscopic effects. In this method, the macroscopic properties of the materials undergoing damage are averaged by relating them to experimentally determined damage variables. MARTIN and CHANDLER [6] performed cyclic loading tests with granite and calculated the relation between strength parameters (friction and cohesion) and damage variables. HAJIABDOLMAJID et al [7] set up a cohesion weakening-friction strengthening (CWFS) model using Mohr-Coulomb failure criterion. In the work of FANG and HARRISON [8−10], the strength degradation behavior of rock is described by a parameter termed degradation index and several degradation models based on the Mohr-Coulomb constitutive law were implemented in FLAC by and them, which reproduced the macroscopic failure process quite well. Based on experimental results on rock specimens in the laboratory, an idealised pressure-sensitive dilatancy model was developed by YUAN and HARRISON [11] to describe the dilatant deformation commonly observed during the brittle fracture of natural rock. ZHAO and CAI [12]

Foundation item: Project(2015M570678）supported by China Postdoctoral Science Foundation funded project,
Received date: 2014−06−20; **Accepted date:** 2014−09−19
Corresponding author: TAN Xin, PhD, Lecturer; Tel: +86−15580373653; E-mail: xintan@hnu.edu.cn

established a mobilized dilation angle model considering the influence of both confining stress and plastic shear strain, which is based on published data acquired from modified triaxial compression tests with volumetric strain measurement.

It is important to understand complete stress−strain relations under different loading conditions and to develop a constitutive model that can adequately represent the complete stress−strain behavior of rock especially for the nonlinear parts including softening and dilation. By the method of CDM models, a modified constitutive law considering the strength degradation and dilation behaviors was developed based on non-linear Hoek-Brown failure criterion [13] in this work. The non-linear degradation and dilation behaviors during progressive failure process of rocks under triaxial compression test can be represented by several internal parameters, which are introduced in this work and related to a certain confining pressure level.

2 Modified constitutive law for brittle rocks

The stress−strain behavior of brittle rocks under compression was subdivided into several stages prior to the macroscopic fracture by ANDREEV [14]: closure of (micro) cracks; linear elastic deformation mainly attributed to the elastic deformation of the grains; stable fracture propagation, the beginning of micro-cracking, obeying Griffith's criterion and the dilation engendered by micro-cracking, adding to the general compaction of the sample; unstable fracture propagation in which crack propagation is independent of σ_1 at this stage, even if the applied load is removed, the cracks could continue their extension because of potential (elastic) energy stored within the body and then the sample compaction ceases and a general volume increase begins; post-failure (post-peak) part can be defined by the onset of remarkable localization up to the macroscopic fracture; residual strength part of which the friction among the pieces (blocks) ensures some bearing capacity of the sample to determine the residual strength.

These processes are particularly difficult to predict and model in the compressive field. This work develops a novel numerical methodology for the simulation of these isolated processes, particularly in compressive fields such that the resulting non-linear macroscopic behaviour can be predicted.

Continuum modeling approach can reproduce a variety of failure phenomena, from brittle fracture to ductile failure and softening behavior by averaging the effect of crack evolution [8]. It should be noticed that almost no continuum hypothesis for failure is based on the real failure mechanism. This model, although is extended and quite complex, it is a phenomenological one and based on a few assumptions: 1) Stress and strain follow a linear elastic relation until peak strength is reached. 2) Peak strength is governed by a single nonlinear failure criterion. 3) Post-failure region is divided into two stages: degradation stage and residual stage. Material strength parameters reduce linearly inside the degradation stage, and are then kept constant at a residual value in the residual stage. 4) The stress−strain relation is governed by certain flow rules in the plastic range. The volumetric response is non-linear and stress depending.

2.1 Elastic stage

This elastic and isotropic model provides the simplest representation of rock behavior that exhibits linear stress−strain behavior with no hysteresis during unloading. The components of stress are linear functions of the components of strain according to following equation [15]:

$$\Delta\sigma_{ij} = 2G\Delta\varepsilon_{ij} + (K - \frac{2}{3})G\Delta\varepsilon_{kk}\delta_{ij} \tag{1}$$

where δ_{ij} is the Kroenecker delta symbol; K is the bulk modulus; G is the shear modulus.

2.2 Failure criterion

For brittle rocks as well as for rock masses, the non-linear Hoek-Brown failure criterion has been proven to give an appropriate description. Over the last decades, this criterion was continuously further developed and applied. The latest version for rock masses is given by following equation [13]:

$$\sigma_1' = \sigma_3' + \sigma_{ci}(m_b \frac{\sigma_3'}{\sigma_{ci}} + s)^a \tag{2}$$

where σ'_1 and σ'_3 are the major and minor effective principal stresses at failure, respectively; σ_{ci} is the uniaxial compressive strength of the intact rock material; m_b, a and s are constants used in Hoek-Brown failure criterion.

2.3 Strength degradation

Rocks exhibit the phenomenon of strain softening under compressive loads. Thereby, the non-linear strength degradation is highly stress-dependent. As documented exemplary by BRADY and BROWN [16], the confining stress strongly influences the shape of the strength degradation as well as the value of residual strength. The strength degradation decreases with increasing confining pressure. Finally, under high confining pressure the rock goes into nearly ductile state and no degradation occurs [6−7, 17].

FANG and HARRISON [8−10] have defined a parameter called degradation index r_d, which controls the variation of the degradation behavior in relation to the confining pressure. The definition of the degradation

index implies that the value for r_d ranges from zero (no degradation associated with ductile behavior) to unity (complete degradation associated with brittle behavior). But only this single parameter cannot represent the relation between degradation rate and confining pressure, and the strength degradation from peak to residual value is not as a gradual process. Therefore, it is necessary to extend the model in such a way that a gradual softening and non-linear failure envelope is included. The simplest approach is to introduce the softening through a linear function. As illustrated in Fig. 1, the rate of strength drop or the slope of the softening stage may be expressed by –tan$s$. Perfectly brittle behavior is characterized by a rate of strength drop close to infinity, whereas perfectly plastic material shows a rate of strength drop close to zero [18].

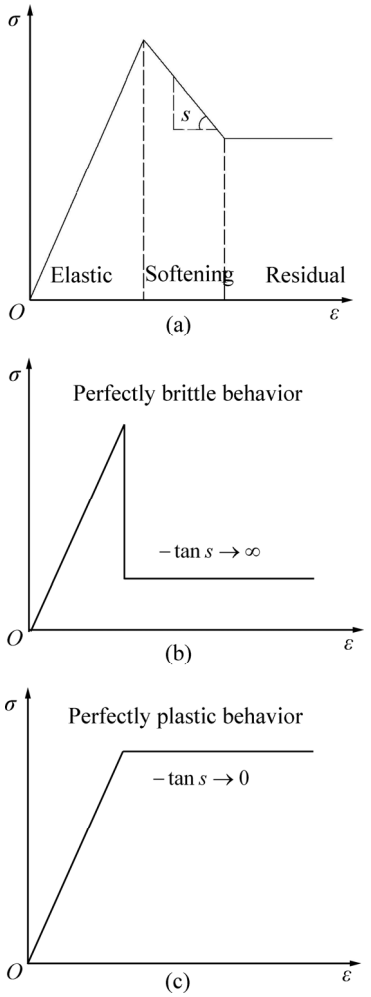

Fig. 1 Strain-softening behavior (a), perfectly brittle behavior (b) and perfectly plastic behavior (c) of rocks [18]

According to the scheme a new degradation model which can represent both strength degradation and degradation drop rate is developed. Figure 2 shows the principle of mechanical strength degradation under different confining pressures. In Fig. 4, σ is the peak stress; $\Delta\sigma$ is the strength degradation; σ_d is the residual

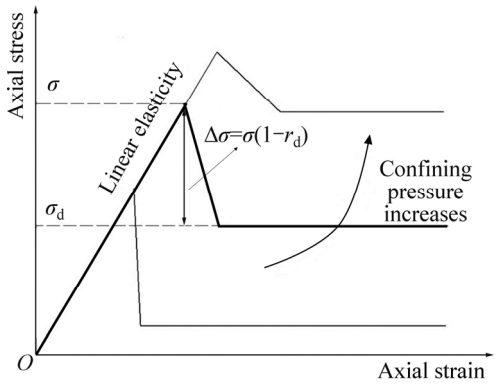

Fig. 2 Idealized constitutive model comprising strength degradation

strength. We define the ratio between $\Delta\sigma$ and σ as the degradation index (r_d).

$$r_d = \frac{\Delta\sigma}{\sigma} \tag{3}$$

The relation between the degradation index and confining pressure can be described by Eq. (4), which is based on laboratory data.

$$r_d = A + B\exp(C\sigma_3) \tag{4}$$

where A, B and C are the fitting parameters, and can be estimated by regression analysis on experimental data.

From the Hoek-Brown failure criterion (Eq. (2)), the peak strength for undisturbed rock and a=0.5 (typical value and approximately valid for most types of rock) can be obtained by Eq. (5):

$$\sigma_1 = \sigma_3 + \sqrt{m_b\sigma_{ci}\sigma_3 + (\sigma_{ci})^2 s} \tag{5}$$

The residual strength parameters can be obtained according to Eq. (6).

$$\begin{aligned}&\sigma_d = \sigma_3 + \sqrt{m_b^d\sigma_{ci}^d\sigma_3 + (\sigma_{ci}^d)^2 s^d}\\ &\sigma_d = \sigma - \Delta\sigma = \sigma(1-r_d) = \sigma_3(1-r_d) + \\ &\qquad \sqrt{m_b(1-r_d)\sigma_{ci}(1-r_d)\sigma_3 + (\sigma_{ci})^2(1-r_d)^2 s}\end{aligned} \tag{6}$$

where σ_{ci}^d, m_b^d and s^d are the residual strength parameters after degradation.

Comparing the two expressions, we can use the degradation index to calculate residual strength parameters according to

$$\begin{cases}\sigma_{ci}^d = \sigma_{ci}(1-r_d)\\ m_b^d = m_b(1-r_d)\\ s^d = s\end{cases} \tag{7}$$

Material softening after the onset of plastic yielding can be simulated by specifying the reduction of the material strength parameters according to a softening parameter. The chosen softening parameter is the plastic strain component e_3^p, which is expected to correlate with

the micro-crack development (damage) in the σ_3 direction [19]. Softening behavior is provided by specifying tables that relate each of the properties σ_{ci}, m_b, s and a to e_3^p, as shown in Fig. 3.

It is assumed that the strength parameters decrease linearly with ongoing plastic strain e_3^p. The degradation rate depends on the accumulated plastic strain Δe_3^p. Moreover, as shown in Fig. 4, increasing confining pressure leads to decreasing accumulated plastic strain Δe_3^p. The investigation of typical laboratory results has revealed that a fitting function according to Eq. (8) is well suited to describe the relation between Δe_3^p and confining pressure:

$$\Delta e_3^p = A_1 + B_1 \exp(C_1 \sigma_3) \tag{8}$$

where A_1, B_1 and C_1 are the fitting parameters, which can be estimated by regression analysis.

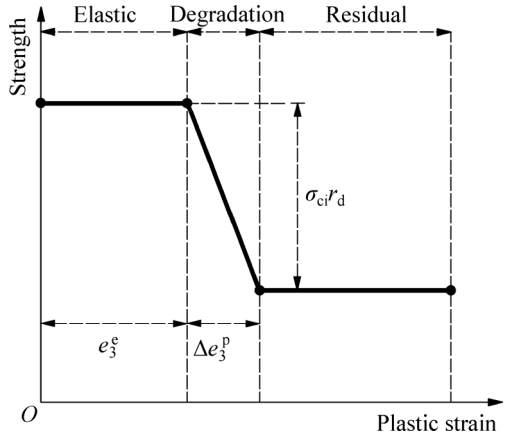

Fig. 3 Scheme of strength degradation

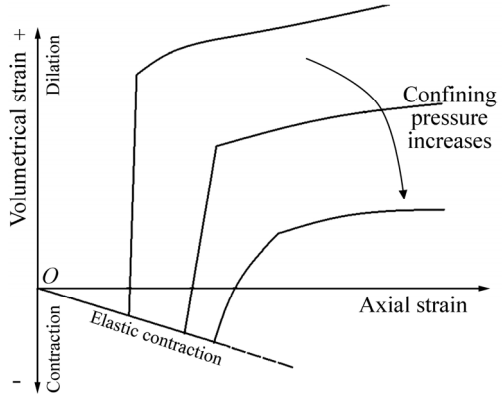

Fig. 4 Idealized elemental constitutive model comprising strength degradation and dilation

2.4 Dilation associated with mechanical degradation

Experimental observations of rock failure show that the failure process is closely associated with rock dilation. Following an initial period of elastic contraction, the volumetric response tends to be dilation as the material enters an inelastic stage that is characterized by the development and coalescence of micro-structural damage [12−13, 17, 20].

When rock is subjected to triaxial compression, the rate of dilation tends to reduce with increasing confining pressure (Fig. 4). We applied a similar approach as the strength degradation, which considers the relationship between dilation and plastic strain component e_3^p, considering the flow rule used for the Hoek-Brown model in FLAC^{3D} [19]. If the yield criterion according to Eq.(2) is violated by stress state, strain increments can be composed of elastic and plastic parts.

$$\begin{cases} \Delta e_1 = \Delta e_1^e + \Delta e_1^p \\ \Delta e_2 = \Delta e_2^e \\ \Delta e_3 = \Delta e_3^e + \Delta e_3^p \end{cases} \tag{9}$$

Note that in FLAC^{3D} plastic flow does not occur in the intermediate principal stress direction. Therefore, the following flow rule is assumed.

$$\Delta e_1^p = \gamma \Delta e_3^p \tag{10}$$

We need to consider an appropriate flow rule, which describes the volumetric behavior of the material during yield. In general, the flow parameter γ will depend on stress, and possibly on stress-deformation history. Three cases are considered below.

Associated flow rule: An associated flow rule is one in which the vector of plastic strain rate is normal to the yield surface.

$$\Delta e_i^p = -\gamma \frac{\partial F}{\partial \sigma_i} \tag{11}$$

Differentiating Eq. (11) by using Eq. (2), one obtains:

$$\begin{cases} \Delta e_1^p = -\gamma \\ \Delta e_2^p = 0 \\ \Delta e_3^p = \gamma[1 + a\sigma_{ci}(m_b \dfrac{\sigma_3}{\sigma_{ci}} + s)^{a-1} \dfrac{m_b}{\sigma_{ci}}] \end{cases} \tag{12}$$

and in combination with Eq. (10):

$$\gamma_{af} = -\frac{1}{1 + a\sigma_{ci}(m_b \dfrac{\sigma_3}{\sigma_{ci}} + s)^{a-1} \dfrac{m_b}{\sigma_{ci}}} \tag{13}$$

Radial flow rule: Under the condition of uni- and multi-axial tensions, we expect that the material would yield in the direction of the tensile tractions. These conditions are fullfilled by the radial flow rule, where the plastic tensile strain vectors are coaxial with the principal stress vectors, so that we obtain:

$$\gamma_{rf} = \frac{\sigma_1}{\sigma_3} \tag{14}$$

Constant-volume flow rule: With increasing

confining stress, a point will be reached, at which the material no longer dilates. A constant-volume flow rule is therefore appropriate when the confining stress is above a user-prescribed level $\sigma_3=\sigma_3^{cv}$. This flow rule is given by

$$\gamma_{cv}=-1 \tag{15}$$

Composite flow rule: We propose to assign the flow rule (and, thus, a value for γ) according to the stress condition. In a pure tensile region, the radial flow rule (γ_{rf}) will be used. For compressive σ_1 and tensile or zero σ_3, the associated flow rule (γ_{af}) is applied. For the interval of $10<\sigma_3<\sigma_3^{cv}$, the value of γ is linearly interpolated between the associated γ_{af} and constant-volume γ_{cv} limits:

$$\gamma=\frac{1}{\frac{1}{\gamma_{af}}+(\frac{1}{\gamma_{cv}}-\frac{1}{\gamma_{af}})\frac{\sigma_3}{\sigma_3^{cv}}} \tag{16}$$

Finally, when $\sigma_3>\sigma_3^{cv}$, the constant volume value, $\gamma=\gamma_{cv}$, is used. It should be noted that, if σ_3^{cv} is set equal to zero, the model will approache a non-associated flow rule with zero dilation angle. If σ_3^{cv} is set to a very high value relative to σ_{ci}, the model will approache an associated flow state. The volumetric response of a compressed cubic element is shown in Fig. 5.

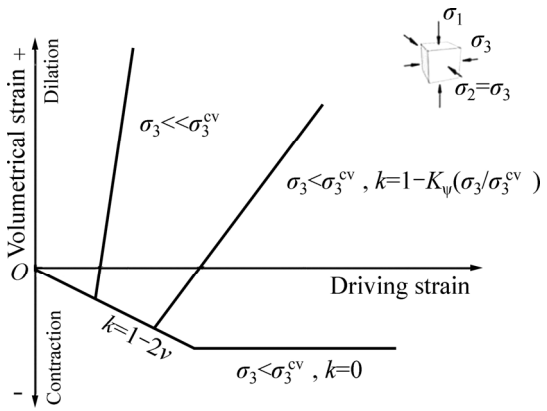

Fig. 5 Principal sketch of volumetric strain vs axial strain

The slope k of curve between volumetric strain and axial strain in the plastic stage depends on the flow parameter γ.

$$k=\frac{\Delta\varepsilon_v^p}{\Delta\varepsilon_1^p}=\frac{\Delta e_1^p+\Delta e_3^p}{\Delta e_1^p}=1+\frac{1}{\gamma} \tag{17}$$

When $\sigma_3>\sigma_3^{cv}$, $\gamma=\gamma_{cv}=-1$ is used and subsequently $k=0$. When $0<\sigma_3<\sigma_3^{cv}$. Eq. (16) is used and the slop k is given by

$$k=1+\frac{1}{\gamma_{af}}+(\frac{1}{\gamma_{cv}}-\frac{1}{\gamma_{af}})\frac{\sigma_3}{\sigma_3^{cv}}=1-K_\psi(\frac{\sigma_3}{\sigma_3^{cv}}) \tag{18}$$

where K_ψ is a parameter which is given by

$$K_\psi(\frac{\sigma_3}{\sigma_3^{cv}})=K_\psi^0(\sigma_3)-\frac{\sigma_3}{\sigma_3^{CV}}[K_\psi^0(\sigma_3)-1] \tag{19}$$

$$K_\psi^0(\sigma_3)=1+\frac{am_b}{(m_b\frac{\sigma_3}{\sigma_{ci}}+s)^{1-a}} \tag{20}$$

The slope k is a function of various parameters σ_{ci}, m_b, s, a, σ_3 and σ_3^{cv}. The strength parameters σ_{ci}, m_b, s and a are constants inside a certain stage. σ_3^{cv} is a user-prescribed stress level in FLAC^{3D}, so that we can control the slope k by setting a suitable value of σ_3^{cv} in the loading process. The volumetric response is represented by fitting the user-prescribed σ_3^{cv} to laboratory observations. Rewriting Eq. (18) and Eq. (20) gives the following expression for σ_3^{cv}, which depends on the minimum principal stress:

$$\sigma_3^{cv}=\frac{\sigma_3[K_\psi^0(\sigma_3)-1]}{k-1+K_\psi^0(\sigma_3)} \tag{21}$$

By replacing the strength parameters and user-prescribed σ_3^{cv} in each stage, slope k can be expressed as (Fig. 6)

$$\begin{cases} k_A=k(\sigma_3,\ \sigma_{ci},\ m_b,\ s,\ (\sigma_3^{cv})_{AB}) \\ k_B=k(\sigma_3,\ \sigma_{ci}^d,\ m_b^d,\ s^d,\ (\sigma_3^{cv})_{AB}) \\ k_B<k_{AB}<k_A \\ k_{BC}=k(\sigma_3,\ \sigma_{ci}^d,\ m_b^d,\ s^d,\ (\sigma_3^{cv})_{BC}) \end{cases} \tag{22}$$

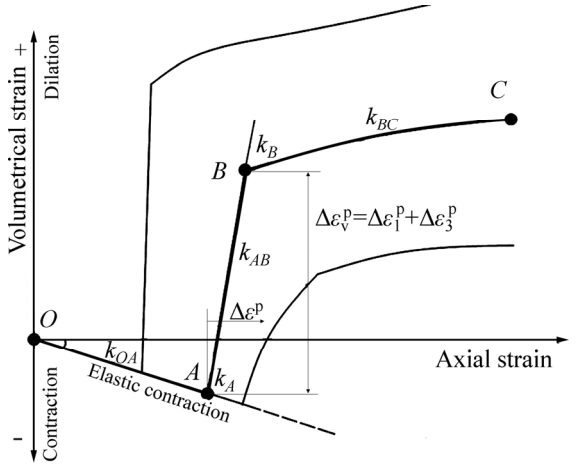

Fig. 6 Sketch of volumetric strains vs axial strain with indication of material parameters

k_{AB} varies linearly between k_A and k_B. $(\sigma_3^{cv})_{AB}$ and $(\sigma_3^{cv})_{BC}$ can be obtained from laboratory observation by using Eqs. (17)−(20). If constant values for $(\sigma_3^{cv})_{AB}$ and $(\sigma_3^{cv})_{BC}$ are assumed under certain confining pressures ranges, the nonlinear dilation curve can be simplified to an analogous-trilinear form. An exponential relation between constant σ_3^{cv} and the minimum principal stress is recommended based on our laboratory observations:

$$\begin{cases}(\sigma_3^{cv})_{AB}=\sigma_3+A_2+B_2\exp(C_2\sigma_3)\\(\sigma_3^{cv})_{BC}=\sigma_3+A_3+B_3\exp(C_3\sigma_3)\end{cases} \quad (23)$$

where A_2, B_2, C_2, A_3, B_3 and C_3 are the fitting parameters, which can be estimated by using linear regression on experimental data.

To sum up, an idealized elemental confining pressure sensitive constitutive model has been developed based on typical laboratory results of granites, which can describe the degradation and the dilation process of brittle rocks.

2.5 Introduction of heterogeneity

Rock is an inhomogeneous material because it consists of many individual components including different minerals, grains, cement materials, voids and cracks. These individual components usually have different physical properties and consequently different responses under different loading conditions. The heterogeneity can be introduced by Weibull distribution [21−22].

A general expression for the Weibull (2-parameter) probability density function can be given by WEIBULL [23−25]:

$$f(x)=\begin{cases}m\beta^m\exp\left[-\left(\dfrac{x}{\beta}\right)^m\right], & x\geq 0\\0, & x<0\end{cases} \quad (24)$$

$$F(x)=\int_0^{+\infty}f(x)\mathrm{d}x=1-\exp\left[-\left(\frac{x}{\beta}\right)^m\right] \quad (25)$$

where x is the random variable that follows the Weibull distribution; m is the shape parameter describing the scatter of x; β is a scale parameter. The mechanical effects of these two parameters were studied in Refs. [26−28].

For the numerical modeling, the basic parameters, such as the uniaxial compressive strength σ_{ci}, the elastic modulus E, follow the Weibull distribution with shape parameter m and scale parameter β. These parameters are assigned to each element of the numerical model randomly. The random spatial distribution of the basic parameters reflects the internal structure (heterogeneity) of material under investigation.

3 Numerical simulation of failure process during triaxial compression test

3.1 Parameters deduced from laboratory results

A stiff (9×10^9 N/m) servo-controlled loading frame (MTS 815) was employed for the triaxial compression tests. Exemplary a complete stress−strain curve is shown in Fig. 7. Typical failure pattern for different confining pressures ranging from 5−30 MPa are shown in Fig. 8. A macroscopic shear fracture penetrates the whole sample after failure of the samples, which is a typical brittle failure characteristic. But the macroscopic shear fracture under high confining stress contains more microcracks, which turns to become more like a plastic shear band [29].

Based on the modified constitutive law a series of parameters (shown in Fig. 7) can be measured using the complete stress−strain curve. The characteristic parameters of Eibenstock II granite under different

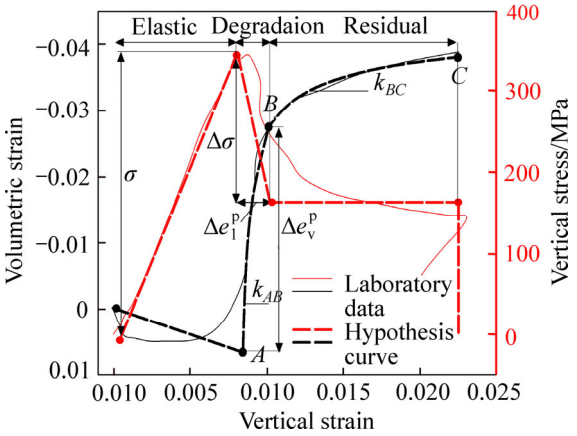

Fig. 7 Complete stress−strain curves with characteristic parameters

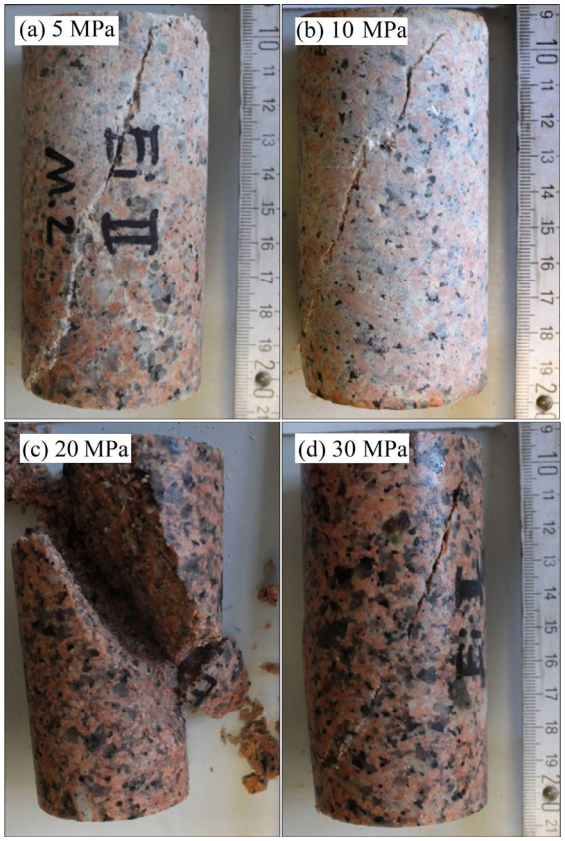

Fig. 8 Failure pattern of Eibenstock II granite samples under different confining pressures: (a) 5 MPa; (b) 10 MPa; (c) 20 MPa; (d) 30 MPa

confining pressures are listed in Table 1 (tested in Rock Mechanical Lab of Geotechnical Institute at TU Bergakademie Freiberg). Notice that r_d, Δe_3^p, $(\sigma_3^{cv})_{AB}-\sigma_3$ and $(\sigma_3^{cv})_{BC}-\sigma_3$ are calculated from the observed parameters σ, $\Delta\sigma$, Δe_I^p, Δe_v^p, k_{AB} and k_{BC}.

The relation between degradation and dilation parameters and confining pressure is set up by empirical relations using exponential fitting equations (Fig. 9) according to the parameters listed in Table 1. The four degradation and dilation parameters decrease with increasing confining pressure, which leads to a peak and residual strength increase and a reduced dilation rate with increasing confining pressure. The mechanical parameters used in the simulations are listed in Tables 2 and 3, where the Hoek−Brown strength parameters were deduced by non-linear fitting function Eq. (2) using the triaxial compression test results.

Table 1 Triaxial parameters of Eibenstock granite samples

σ_3/MPa	σ_1/MPa	$\Delta\sigma$/MPa	r_d	Δe_I^p /%	Δe_v^p /%
0	110	100	0.9	1.00×10^{-3}	10
5	180	130	0.72	8.30×10^{-2}	7.5
10	260	150	0.58	0.15	5.3
20	340	170	0.5	0.3	4
30	430	170	0.4	0.4	3.4

Δe_3^p /%	k_{AB}/	k_{BC}/	$((\sigma_3^{cv})_{AB}-\sigma_3)$/ MPa	$((\sigma_3^{cv})_{BC}-\sigma_3)$/ MPa
10	/	/	300	200
7.4	90	3.3	195	75
5.15	34	2.3	140	25
3.7	13	0.77	90	10
3	8.5	0.56	70	8

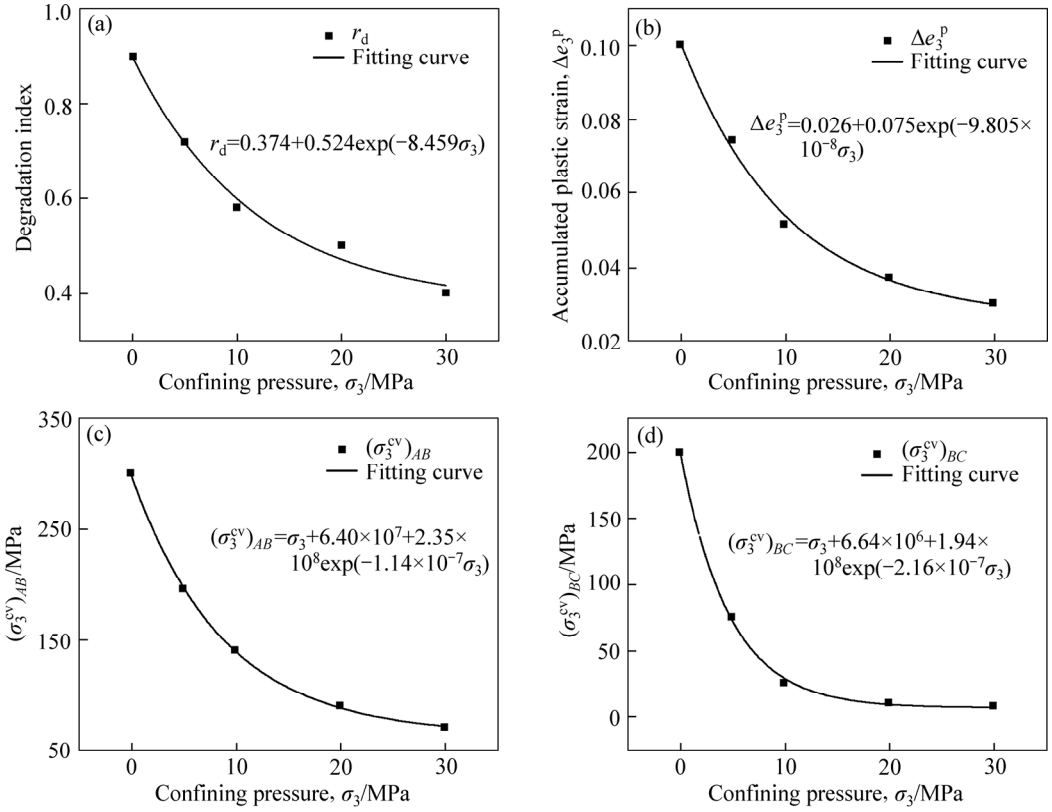

Fig. 9 Observed degradation and dilation parameters at different confining pressures and corresponding fitting curves: (a) Degradation index; (b) Accumulated plastic strain; (c) $(\sigma_3^{cv})_{AB}$; (d) $(\sigma_3^{cv})_{BC}$

Table 2 Mechanical parameters determined from lab test results

Elastic modulus, E/GPa	Poisson ratio, ν	Uniaxial compressive strength, σ_{ci}/MPa	Hoek−Brown parameter			Distribution parameter	
			m_b	s	a	m	β
31	0.26	106	42	0.8	0.5	20	1.05

Table 3 Fitting parameters for lab test results (based on SI units)

A	B	C	A_1	B_1	C_1	A_2	B_2	C_2	A_3	B_3	C_3
0.37	0.52	−8.46	0.026	0.075	-9.8×10^{-8}	6.4	2.35	-1.14×10^{-7}	6.64	1.94	-2.16×10^{-7}

3.2 Numerical simulation results compared with lab test results

Via the internal program language FISH the modified constitutive law combined with heterogeneous parameter distribution was implemented into the numerical code FLAC^{3D} and a numerical simulation scheme was developed (Fig. 10).

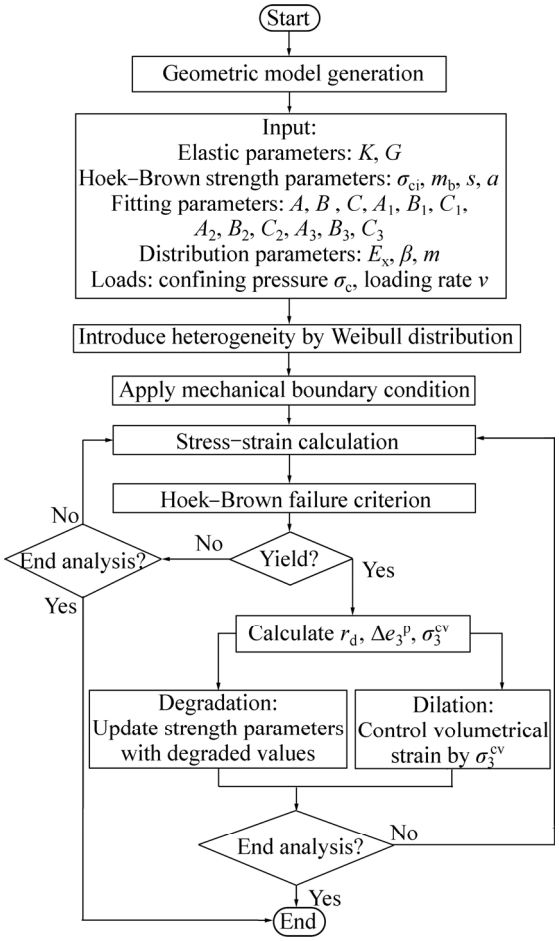

Fig. 10 Scheme of numerical simulation procedure

A series of 3-dimensional numerical simulations of triaxial compression tests were conducted with FLAC^{3D}. The model has a height of 100 mm and a diameter of 50 mm. The mesh contains 96000 elements and 100521 grid-points. A constant grid-point velocity of 5×10^{-8} m/step was applied at the top and bottom of the sample, respectively. During the simulation of the triaxial loading process the elements deform and reveal degradation and dilation. Considering the strength heterogeneity, the elements undergoing degradation and dilation will coalesce and then lead to the formation of macroscopic fractures. The simulated stress−strain curves under confining pressure of 20 MPa are shown in Fig. 11. Figures 12−13 display the fracture development and deformation evolution during the failure process for the selected loading points 1−10 as marked in Fig. 11.

Some conclusions can be drawn from the simulated failure process. 1) During the elastic deformation stage

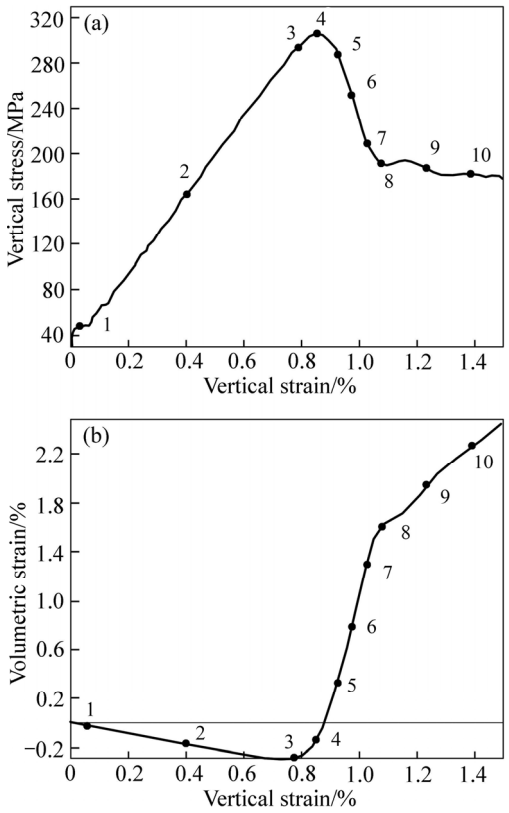

Fig. 11 Simulated stress−strain curve for triaxial compression test under confining pressure of 20 MPa: (a) Vertical stress−strain curve; (b) Volumetric strain−vertical strain curve

from points 1 to 3 nearly no damage happened; the volumetrical strain in every element is negative (compressive); no plastic shear strain happened; the principle stresses are homogeneously distributed and the displacement vectors are vertical. 2) Near peak load around point 4, a few elements begin to degrade. 3) After the peak load from points 4 to 8 more and more elements lost their initial strength; the volumetrical strain turned into the positive range (dilation); plastic shear strain increased, which means that elements show shear failure. The whole sample was in the degradation stage until point 8; the most damaged elements formed the shear band; the displacement vectors are oriented in different directions (development of "blocks" with different movement direction). 4) From point 8 to point 10 the sample is in the residual stage; new macroscopic fractures are not generated, but volumetric strain and plastic shear strain continuously increasd and the shear band became wider.

Several observation points were chosen to track the volumetric response in different parts of the sample, which shows the localization during the loading process. The recorded volumetric strain evolution is shown in Fig. 14. The macroscopic fracture patterns for samples under different confining pressures in 3D view are shown in Fig. 15.

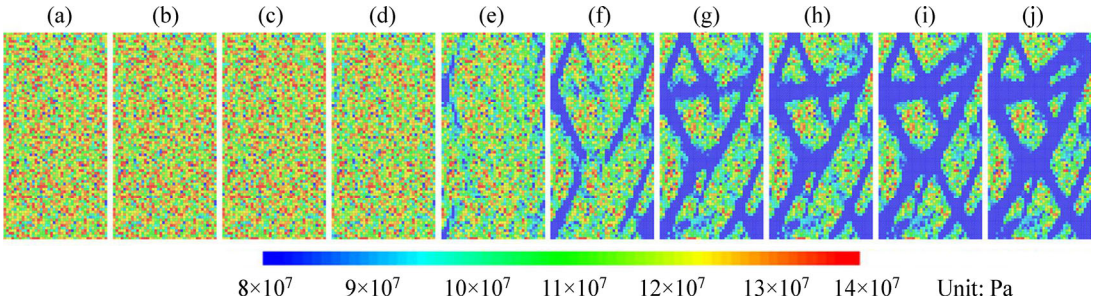

Fig. 12 Uniaxial compressive strength evolution in simulated triaxial compression test under confining pressure of 20 MPa

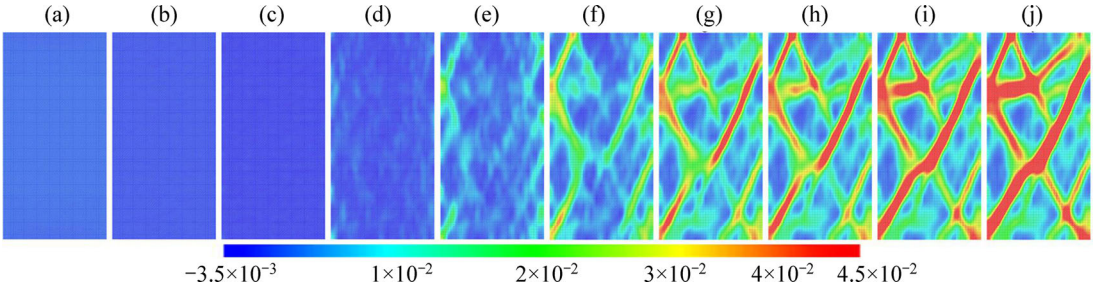

Fig. 13 Volumetric strain evolution in simulated triaxial compression test under confining pressure of 20 MPa

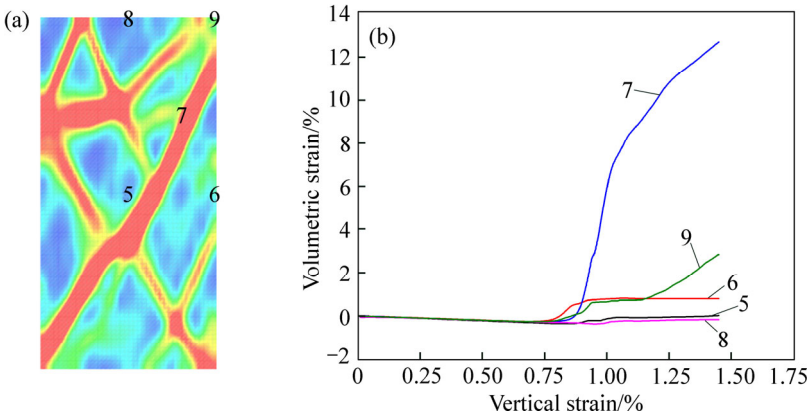

Fig. 14 Volumetrical strain evolution in different parts of sample: (a) Strain distribution; (b) Strain evolution at marked points

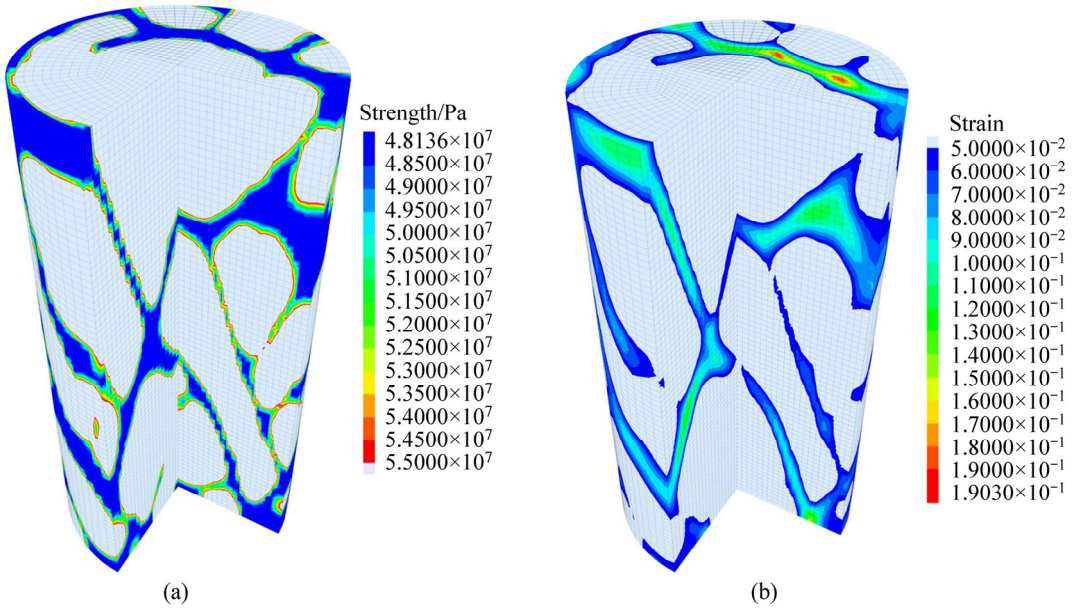

Fig. 15 Macroscopic fracture patterns for samples in 3D view: (a) Degraded uniaxial compressive strength at point 10 (σ_{ci}<5.5×10^7 Pa); (b) Volumetrical strain at point 10 (ε_v>5%)

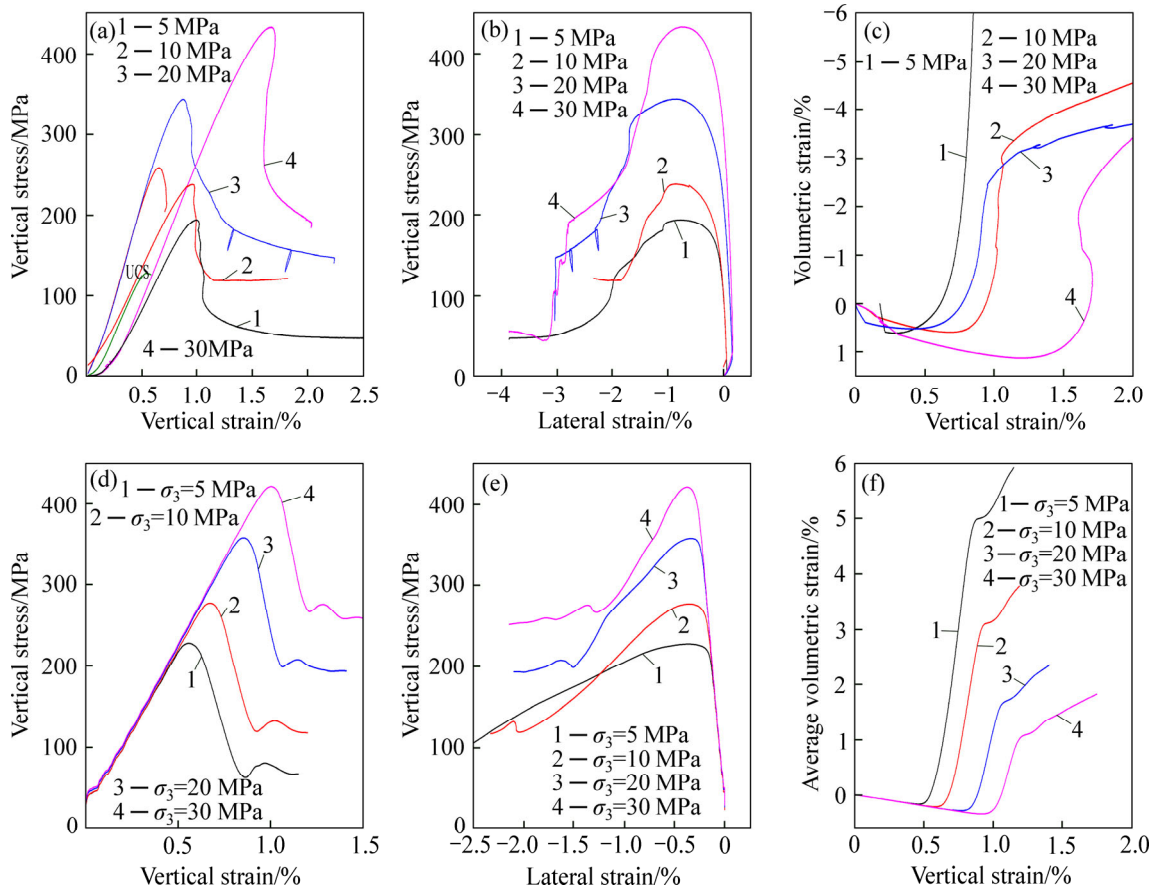

Fig. 16 Complete set of stress−strain curves for different confining pressures compared with lab results: (a, b, c) Lab results; (d, e, f) Simulation results

The complete stress−strain curves obtained from numerical simulations and lab test results under different confining pressures are shown in Fig. 16. A good agreement was found between the numerical simulation results and the laboratory measurements, especially in quantitative description of the peak strength, residual strength and volumetrical strain. But still, the uncertainty caused by natural rock samples is out of the capability of numerical numerical simulations.

4 Conclusions

By analyzing the complete stress−strain curves obtained by triaxial compression tests, the failure process for granite (brittle material) is studied. Based on experimental results on rock specimens in the laboratory, a modified constitutive model is developed which follows the principles of the continuum damage mechanics method. It incorporates non-linear Hoek−Brown failure criterion, confining pressure-dependent strength degradation and volume dilation laws, and is able to represent the nonlinear degradation and dilation behaviors of brittle rocks in the post-failure region. The strength degradation after the onset of plastic yielding is quantitatively described by a degradation index r_d, and the softening behavior can be obtained by specifying the reduction of the Hoek−Brwon strength parameters according to the plastic strain component e_3^p, which is expected to correlate with the micro-crack development (damage) in the σ_3 direction. The dilation behavior can be adjusted by setting a appropriate user-prescribed stress e_3^{cv}, which is a parameter to control plastic strain used in FLAC^{3D}. By relating the degradation index r_d and user-prescribed stress e_3^{cv} to the confining pressure, the confining pressure-dependent failure behavior can be represented. With the increase of confining pressure, the ductile characteristics of rock become more obvious, plastic deformation as well as peak and residual strength are enhanced, and finally the volume dilation tends to become stable. Via the internal program language FISH, the modified constitutive law combined with heterogeneous parameter distribution is implemented into FLAC^{3D} and a numerical simulation scheme is developed. Using the new developed modified constitutive law, a good agreement is found between the numerical simulation results and the laboratory measurements, which shows that the modified constitutive law is appropriate to describe the complete material behavior of brittle rocks including the post failure stage.

References

[1] OFOEGBU G I, CURRAN J H. Deformability of intact rock [J]. Int J Rock Mech Min Sci Geomech Abstr, 1992, 29(1): 35−48.

[2] KRAJCINOVIC D, FONSEKA G U. The continuous damage theory of brittle materials—Part 1: general theory [J]. J Appl Mech Trans ASME, 1981, 48: 809−815.

[3] COSTIN L S. Damage mechanics in the post-failure regime [J]. Mech Mater, 1985, 4: 149−160.

[4] BASISTA M, GROSS D. The sliding crack model of brittle deformation: An internal variable approach [J]. Int J Solids Struct, 1998, 35(5/6): 487−509.

[5] YUAN S C, HARRISON J P. A review of the state of the art in modelling progressive mechanical breakdown and associated fluid flow in intact heterogeneous rocks [J]. International Journal of Rock Mechanics and Mining Sciences, 2006, 43(7): 1001−1022.

[6] MARTIN C D, CHANDLER N A. The progressive fracture of Lac du Bonnet granite [J]. International Journal of Rock Mechanics and Mining Sciences and Geomechanics Abstracts, 1994, 31(6): 643−659.

[7] HAJIABDOLMAJID V, KAISERAR P K, MARTIN C D. Modelling brittle failure of rock [J]. International Journal of Rock Mechanics and Mining Sciences, 2002, 39(6): 731−741.

[8] FANG Z, HARRISON J P. A mechanical degradation index for rock [J]. International Journal of Rock Mechanics and Mining Sciences, 2001, 38(8): 1193−1199.

[9] FANG Z, HARRISON J P. Development of a local degradation approach to the modelling of brittle fracture in heterogeneous rocks [J]. International Journal of Rock Mechanics and Mining Sciences, 2002, 39(4): 443−457.

[10] FANG Z, HARRISON J P. Application of a local degradation model to the analysis of brittle fracture of laboratory scale rock specimens under triaxial conditions [J]. International Journal of Rock Mechanics and Mining Sciences, 2002, 39(4): 459−476.

[11] YUAN S C, HARRISON J P. An empirical dilatancy index for the dilatant deformation of rock [J]. International Journal of Rock Mechanics and Mining Sciences, 2004, 41(4): 679−686.

[12] ZHAO X G, CAI M. A mobilized dilation angle model for rocks [J]. International Journal of Rock Mechanics and Mining Sciences, 2010, 47(3): 368−384.

[13] HOEK E, CARRANZA-TORRES C, CORKUM B. Hoek-Brown criterion-2002 edition [C]// Proc NARMS-TAC Conference. Toronto, 2002, 1: 267−273.

[14] ANDREEV G E. Brittle failure of rock materials: Test results and constitutive models [M]. (1st ed) Rotterdam: Taylor & Francis, 1995.

[15] HUDSON J A, HARRISON J P. Engineering rock mechanics—An introduction to the principles [M]. (4th ed) Amsterdam: Elsevier Ltd, 2005.

[16] BRADY B H G, BROWN E T. Rock mechanics for underground mining [M]. (2nd ed) London: Chapman & Hall, 1992.

[17] KARSTUNEN M, PANDE G N, DESRUES J. Strain localisation and rotation of principal stress axis in biaxial test [C]// Proc 9th Conference of Computer Methods and Advances in Geomechanics. Wuhan, 1997.

[18] ALONSO E, ALEJANO L R, VARAS F, FDEZ-MANIN G, CARRANZA-TORRES C. Ground response curves for rock masses exhibiting strain-softening behavior [J]. International Journal for Numerical and Analytical Methods in Geomechanics, 2003, 27(13): 1153−1185.

[19] Itasca Consulting Group, Inc. FLAC3D fast lagrangian analysis of continua in 3 dimensions-theory and background [M]. Minneapolis: Itasca Consulting Group Inc, 2006.

[20] LADANYI B, ARCHAMBAULT G. Simulation of shear behaviour of a jointed rock mass [C]// The 11th U.S. Symposium on Rock Mechanics. Berkeley: American Rock Mechanics Association, 1969.

[21] CHEN S, YUE Z Q, THAM L G. Digital image-based numerical modeling method for prediction of inhomogeneous rock failure [J]. International Journal of Rock Mechanics and Mining Sciences, 2006, 41(6): 939−957.

[22] CHEN Sha, YUE Zhong-qi, THAM L G. Actual mesostructure based three-dimensinal numerical modeling, method for heterogeneous geomaterials [J]. Chinese Journal of Rock Mechanics and Engineering, 2006, 25(10): 1951− 1959. (in Chinese)

[23] WEIBULL W A. Statistical distribution function of wide applicability [J]. Journal of Applied Mechanics, 1954, 18: 293−297.

[24] BLAIR S C, COOK N G W. Analysis of compressive fracture in rock using statistical techniques: Part I. A non-linear rule—based model [J]. Int J Rock Mech Min Sci, 1998, 35: 837−848.

[25] CAO Wen-gui, ZHAO Ming-hua, LIU Cheng-xue. Study on the model and its modifying method for rock softening and damage based on Weibull random distribution [J]. Chinese Journal of Rock Mechanics and Engineering, 2004, 23(19): 3226−3231. (in Chinese)

[26] LIU H, ROQUETE M, KOU S Q, LINDQVIST P A. Characterization of rock heterogeneity and numerical verification [J]. Engineering Geology, 2004, 72(1/2): 89−119.

[27] FENG X T, PAN P Z, ZHOU H. Simulation of the rock micro-fracturing process under uniaxial compression using an elasto-plastic cellular automaton [J]. International Journal of Rock Mechanics and Mining Sciences, 2006, 43(7): 1091−1108.

[28] HUET C. An integrated micromechanics and statistical continuum thermodynamics approach for studying the fracture behavior of microcracked heterogeneous materials with delayed response [J]. Engineering Fracture Mechanics, 1997, 58(5/6): 459−556.

[29] TAN X, KONIETZKY H. Laboratory observation and numerical simulation of permeability evolution during progressive failure of brittle rocks [J]. International Journal of Rock Mechanics & Mining Sciences, 2014, 68: 167−176.

(Edited by YANG Hua)